Mar Geophys Res (2007) 28:127–138
DOI 10.1007/s11001-007-9020-y

ORIGINAL RESEARCH PAPER

Low-amplitude BSRs and gas hydrate concentration on the northern margin of the South China Sea

Shiguo Wu · Xiujuan Wang · How Kin Wong · Guangxue Zhang

Received: 29 May 2006 / Accepted: 27 April 2007 / Published online: 19 June 2007

Abstract The passive northern continental margin of the South China Sea is rich in gas hydrates, as inferred from the occurrence of bottom-simulating reflectors (BSR) and from well logging data at Ocean Drilling Program (ODP) drill sites. Nonetheless, BSRs on new 2D multichannel seismic reflection data from the area around the Dongsha Islands (the Dongsha Rise) are not ubiquitous. They are confined to complex diapiric structures and active fault zones located between the Dongsha Rise and the surrounding depressions, implying that gas hydrate occurrence is likewise limited to these areas. Most of the BSRs have low amplitude and are therefore not clearly recognizable. Acoustic impedance provides information on rock properties and has been used to estimate gas hydrate concentration. Gas hydrate-bearing sediments have acoustic impedance that is higher than that of the surrounding sediments devoid of hydrates. Based on well logging data, the relationship between acoustic impedance and porosity can be obtained by a linear regression, and the degree of gas hydrate saturation can be determined using Archie's equation. By applying these methods to multichannel seismic data and well logging data from the northern South China Sea, the gas hydrate concentration is found to be 3–25% of the pore space at ODP Site 1148 depending on subsurface depth, and is estimated to be less than values of 5% estimated along seismic profile 0101. Our results suggest that saturation of gas hydrate in the northern South China Sea is higher than that estimated from well resistivity log data in the gas hydrate stability zone, but that free gas is scarce beneath this zone. It is probably the scarcity of free gas that is responsible for the low amplitudes of the BSRs.

Keywords Bottom simulating reflectors · Gas hydrates · Free gas · Saturation · South China Sea

S. Wu (✉) · X. Wang
Institute of Oceanology, Chinese Academy of Sciences, Qingdao, China
e-mail: swu@ms.qdio.ac.cn

S. Wu · X. Wang
Key Laboratory of Marine Geology and Environment, Chinese Academy of Sciences, Qingdao, China

H. K. Wong
Institute of Biogeochemistry and Marine Chemistry, University of Hamburg, 20146 Hamburg, Germany

G. Zhang
Guangzhou Marine Geological Survey, MLR, Guangzhou 510760, China

Introduction

A bottom simulating reflector (BSR) generally marks the base of the gas hydrate stability zone in marine sediment and is the most important geophysical expression of marine gas hydrates (Shipley et al. 1979; Hyndman and Spence 1992; Minshull et al. 1994). Thus, multichannel seismic data has been used to estimate the quantity and distribution of gas hydrates and associated free gas (Andreassen 1995; Hyndman and Davis 1992; Lee et al. 1994; Paull and Dillon 2001; Sloan 1998; Yuan et al. 1996). Since 1999, high-resolution multichannel seismic surveys have been carried out for gas hydrate resource studies in the northern South China Sea. BSRs were discovered successively in the Xisha Trough, on the Dongsha Rise and in the Taixinan Basin of the northern South China Sea (Chi et al. 1998; Song et al. 2001; Wang et al. 2003; Wu et al. 2005; Yao 2001; Zhang et al. 2002; see Fig. 1). Estimates of gas hydrate quantity and distribution have been made (Chi et al.

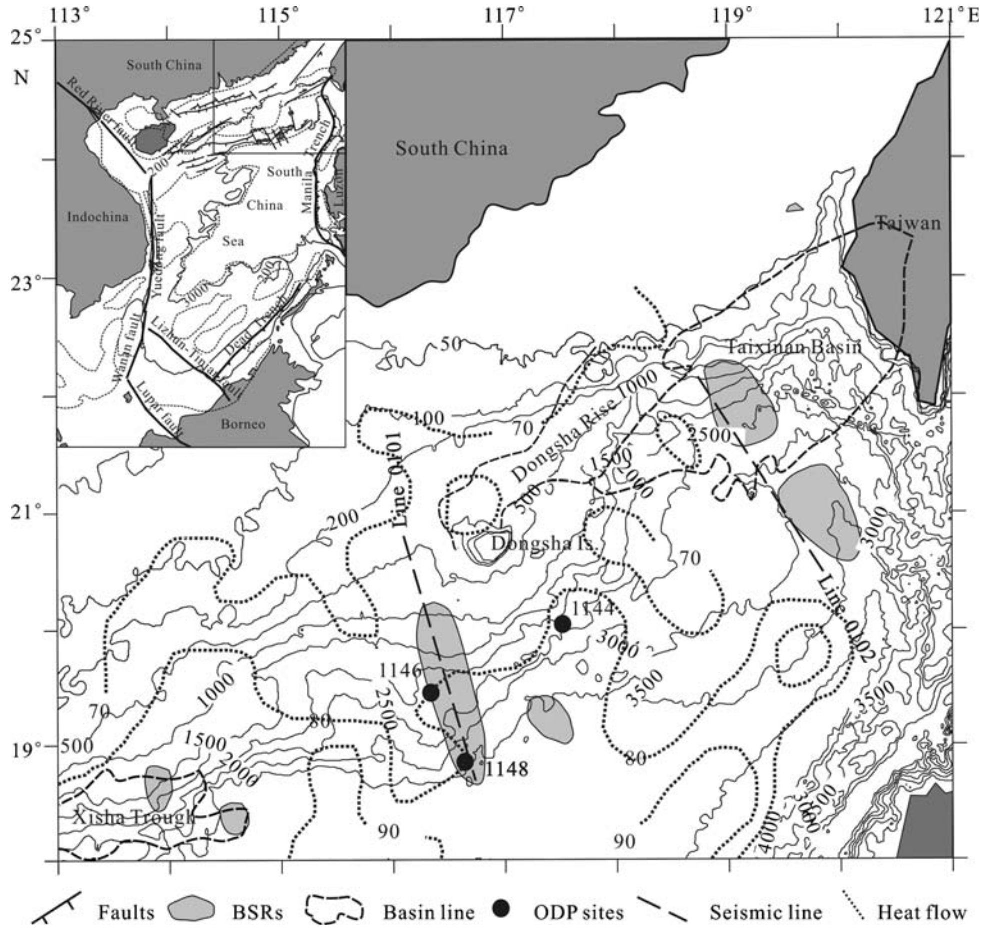

Fig. 1 Structural and bathymetric map of the northern South China Sea showing the distribution of BSRs. Dotted lines give the locations of the seismic profiles used in this study and those parts depicted in Figs. 2–4 are shown as thick lines. Dots indicate ODP Leg 184 drill sites. Inset shows major faults (after Lüdmann and Wong 1999) and subduction zones in the South China Sea. Heat flow from Shi et al. (2003)

1998; McDonnel et al. 2000; Yao 1998, 2001; Zhang et al. 2002). The South China BSRs are heterogeneous in character and are limited to local areas even though methane hydrate is stable under the prevalent thermobaric conditions at water depths of 550–3000 m here (Jin and Wang 2002), While these resource estimates are probable rough they do allow approximations to be made of the gas hydrate saturation, distribution and the effect of sediment porosity. Factors such as water depth, temperature, origin and composition of the gaseous hydrocarbons and geological structure are favourable for the formation of gas hydrates in most parts of the northern South China Sea, but the BSRs discovered occur only in the form of ribbons or sheets locally, a fact which has been ascribed to the association with specific active structural features and rugged sea bottom morphology (Wang et al. 2003; Wu et al. 2005).

The worldwide distribution of submarine gas hydrates suggests that tectonics plays an important role in their formation and accumulation. Milkov (2000) showed that structures such as active fault systems, mud volcanoes and other tectonic pathways control gas migration and gas hydrate accumulation. Gas hydrates are abundant, for example, on the continental slope of the Gulf of Mexico (Dai et al. 2004; McConnell and Kendall 2003), at Hydrate Ridge Offshore Oregon (Milkov et al. 2003), in the Black Sea and offshore West Africa. Egeberg (2000) pointed out that ODP Site 996 on the Blake Ridge is located above a diapiric structure with numerous indications for vertical fluid migration and hydrate occurrence. The relationships between tectonics and BSR distribution on the passive margin of the northern South China Sea are poorly known (Wang et al. 2003; Wu et al. 2005). These need investigation in order to better search for, identify and interpret BSRs and to better estimate the quantity of gas hydrates present. In this paper, we discuss the relationship between geological structure and distribution of BSRs and estimate gas hydrate concentration on the passive margin of the northern South China Sea using high-resolution multichannel seismic profiles.

Geological setting

The South China Sea is one of the largest marginal seas in the western Pacific (Fig. 1). The South China Sea was formed by oceanic spreading along a WSW-ENE axis during the Oligo-Miocene (Briais et al. 1993; Lee and Lawver 1995; Taylor and Hayes et al. 1983) although the origin of the extensional forces is controversial. The structure of its northern margin has been extensively studied in the course of oil exploration and geophysical investigations concerning the amount of crustal extension during the opening of its Central Basin (e.g., Clift et al. 2002; Clift and Lin 2001). Sedimentary basins in the South China Sea contain over 4 km of Cenozoic deposits that have been drilled during hydrocarbon exploration and imaged by seismic data (Lüdmann et al. 2001). The present shape of the South China Sea is closely associated with the relative motion of the Philippine Sea plate to the east and the ongoing collision with the Indo-Australian plate to the south. The northern South China Sea is a passive continental margin formed prior to and during the Middle Oligocene-Early Miocene opening of the Central Basin (32–17 Ma: Briais et al. 1993; Clift et al. 2002). Counter-clockwise rotation of the Philippine Sea plate has led to arc-continent collision between the underthrusting Eurasian plate and the Luzon Arc in the region of Taiwan since 6.5 Ma (Huang et al. 1997).

The northern slope of the South China Sea with a total area of about 2.3×10^5 km^2 has a length of 900 km and a width ranging between 143 and 342 km, widening from east to west. The water depth varies from 150 to 3700 m, and the angle of slope is 0.7–1.3°. The stepwise morphology of the northern slope is controlled by fault systems striking NE-SW, E-W and NW-SE respectively. On this slope, a variety of physiographic features, such as troughs, seamounts, scarps, platforms, incised valleys and fan channels are well developed. Sediments deposited since the Late Oligocene belong to fluvial, lacustrine, deltaic, shallow marine and bathyal facies. They are characterized by high accumulation rates in the Oligocene, low accumulation rates and high carbonate content from the Middle Miocene to the Early Pliocene, and high accumulation rates and a low carbonate content in the Late Pliocene-Recent (Wang et al. 2000). But there is a controversy about the history of sedimentation. Clift (2006) suggested that the sharp increase in sedimentation rates in East Asia after 33 Ma possibly reflected strong surface uplift of the Tibetan plateau and/or intensification of the Asian monsoon. The total organic carbon content (TOC) in the late Cenozoic sediments is 0.2–1.1% (Zhu et al. 2003; Leventhal 2004), while total organic carbon content (TOC) of 300 sediment samples from the upper 150 m section of ODP Site 1146 is 0.36–1.88%. Distinct hydrocarbon anomalies include the occurrence of biogenic methane at ODP Site 1144 and of thermal gases (including methane, ethane, dimethylmethane and macromolecular hydrocarbons) in the Miocene strata at ODP Site 1146. Thus, gaseous hydrocarbons are plentiful and conditions are favourable for gas hydrate generation in the northern South China Sea (Zhu et al. 2003).

Two fault systems striking NE-SW and NW-SE are well-developed in the northern South China Sea (Lüdmann and Wong 1999). In our study area, the NE to ENE-striking fault system dominates. Fault formation and magma intrusion along the fault zones occurred during the Upper Cretaceous to Paleogene rifting and Late Oligocene to Miocene seafloor spreading of the South China Sea. Some of these faults in the east were reactivated during the Pliocene and the Quaternary because of the subduction and subsequent collision of the Philippine plate with the Eurasian plate along the Luzon arc (Huang et al. 1997).

Geophysical expressions of gas hydrate occurrence in the northern South China Sea

Data description

The multichannel seismic (MCS) profiles we used for this study (Fig. 1) were shot by the Guangzhou Marine Geological Survey. Seismic line 0102 was shot in July, 2002 by ''FEN DOU WU HAO'', using a long streamer with 192 channels (trace interval 12.5 m) and coherent airgun sources with volume 8 x 20 in^3 shooting every 25 m. The sampling interval was 1 ms. Streamer depth was 6 m and source depth was 2 m. Seismic line 97301 was shot in April, 2001 by ''TAN BAO HAO'', using a 3000-m-long streamer with 240 channels (trace interval 12.5 m) and a shot interval of 50 m. The sample interval is 2 ms and the depth of source is 8 m. Seismic line 0101 was shot in November 2001 by ''FEN DOU WU HAO'' with 96 channels (trace interval 12.5 m) with a shot interval of 25 m. The sample interval is 1 ms. The source depth was 2 m and streamer depth was 6 m.

The data were processed by the Institute of Processing, Guangzhou Marine Geological Survey. The processing sequences mainly contained pre-filter, true amplitude recover, noise attenuation, deconvolution, velocity analysis (first), residual statics, velocity analysis (second), multiple attenuation, dip moveout velocity analysis, dip moveout stack and noise attenuation.

Hydrate stability field

Heat flow in South China Sea has been studied since 1970, while most of the data were obtained after 1980. Anderson et al. (1978) compiled all the heat flow data measured in 1970's. Heat flow values over the northern South China Sea are shown in Fig. 1 (Shi et al 2003). Thermal conductivity measurements at ODP Site 1148 are presented in Fig. 2a. The data range from 0.85 to 1.30 W/m K. The downhole temperature gradient at ODP Site 1148 was calculated using the following equation (Shipboard Party 2000):

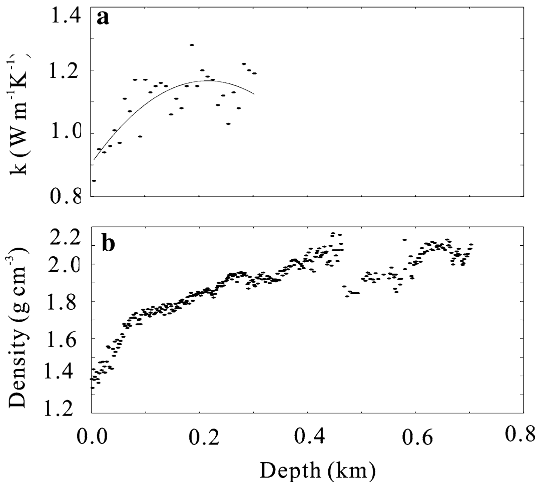

Fig. 2 (**a**) Variation of thermal conductivity with depth below seafloor. (**b**) Density model used in heat flow calculations to estimate the lithostatic pressure at the BSR

$$T(^\circ\mathrm{C}) = 3.48 + 0.084 \times z \tag{1}$$

where z is the depth below seafloor in m. The temperature of seafloor is 3.48°C.

The temperature at the BSR depth (T_{bsr}) was determined from the pressure–temperature stability conditions for methane hydrate by Dickens and Quinby-Hunt (1994):

$$\frac{1}{T} = 3.79 \times 10^{-3} - 2.83 \times 10^{-4} \log(P) \tag{2}$$

Where T is the temperature in K and P is the lithostatic pressure in MPa. The lithostatic pressure was determined using a density model (Fig. 2b) based on measurements taken from core at ODP Site 1148. A water density of 1.05 g/cm^3 is assumed. In the first interval (0–46 meters composite depth (mcd)), the bulk density increases linearly from 1.3 g/cm^3 at the seafloor to 1.4 g/cm^3. In the second interval, density is greater than in the first interval and increases from 1.4 to 1.6 g/cm^3 at 88 mcd. In the third interval (88–457 mcd), density increases gently from 1.6 g/cm^3 to 1.9 g/cm^3 (Shipboard Party 2000). The temperature at the BSR depth (T_{bsr}) calculated by Eq. 2 is not sensitive to the bulk density.

An empirical expression giving the average thermal conductivity (k) from ODP Site 1148 was determined by smoothly fitting the data with a low order polynomial (Fig. 2a):

$$k = 0.9018 + 0.0025z - 6.0 \times 10^{-6} z^2 \tag{3}$$

where k is the thermal conductivity in W/(m K) and z is the depth below the seafloor in m.

Fig. 3 (**a**) Part of seismic profile 0101 across ODP Site 1148; (**b**) The acoustic impedance distribution along part of profile 0101 obtained by CSSI. (**c**) The corresponding porosity section obtained from the acoustic impedance section using Eq. 9; (**d**) The corresponding gas hydrate saturation section estimated using the porosity section shown in (c), Eq. 8 and appropriate numerical values for the parameters m, a and n in the gas hydrate zone. See text for discussions. The interpreted low-amplitude BSR is marked by a dotted line. Site 1148 is the ODP Leg 184 drill site. See Fig. 1 for profile location

Heat flow values (H) were calculated using the simple conductive heat transport relation:

$$H = k \frac{T_{bsr} - T_{sea}}{z_{bsr}} \tag{4}$$

Heat flow at this area (Fig. 1) is about 70 mW/m^2 (Clift and Lin 2001; Shi et al. 2003). The stability depth of BSR at ODP Site 1148 can be calculated using Eqs. 2–4 to be at a depth of about 305 m.

Low-amplitude BSRs

In the northern South China Sea, BSRs are generally parallel to the seafloor and to the sediment stratification, making them difficult to recognize. However, blanking zones, high-amplitude zones, as well as phase reversals can be helpful indicators of the presence of gas hydrates. Fig. 3a shows seismic line 0101, which crosses ODP Site 1148 (18°50'N, 116°34'E; water depth: 3295 m; drilled to 853 mbsf) on the lower slope west of the Dongsha Rise. The concentration of carbonate ranges from 1% to 76%. High carbonate concentration from 300 to 476 mbsf caused high velocity on this profile (1.8–2.0 km/s, 0.2 km/s higher than corresponding values on the Blake Ridge). TOC decreases systematically from a maximum of 0.8 wt% at the seafloor to 0.2 wt% at 130 mcd (Shipboard Party 2000). The blanking zone has a thickness of about 0.4 s TWT, although the blanking effect is so weak that strata are almost visible within this zone. A BSR with a polarity reverse to that of the seafloor can be discerned at the base of the blanking zone, but its amplitude is low and it is subparallel to the seafloor. A high-amplitude zone is absent on this profile (Song 2003; Wu et al. 2005).

Fig. 4a shows seismic line 0102 located east of the Dongsha Islands. The BSR on this profile is more readily recognizable than on line 0101, which may be a result of the occurrence of several interpreted normal faults in the basement, numerous small faults in the upper part of the section, and a diapiric structure at CDP 12481–12956.

Constrained sparse spike inversion

Compressional velocity analysis and Amplitude Versus Offset (AVO) analysis of hydrated sediments are well

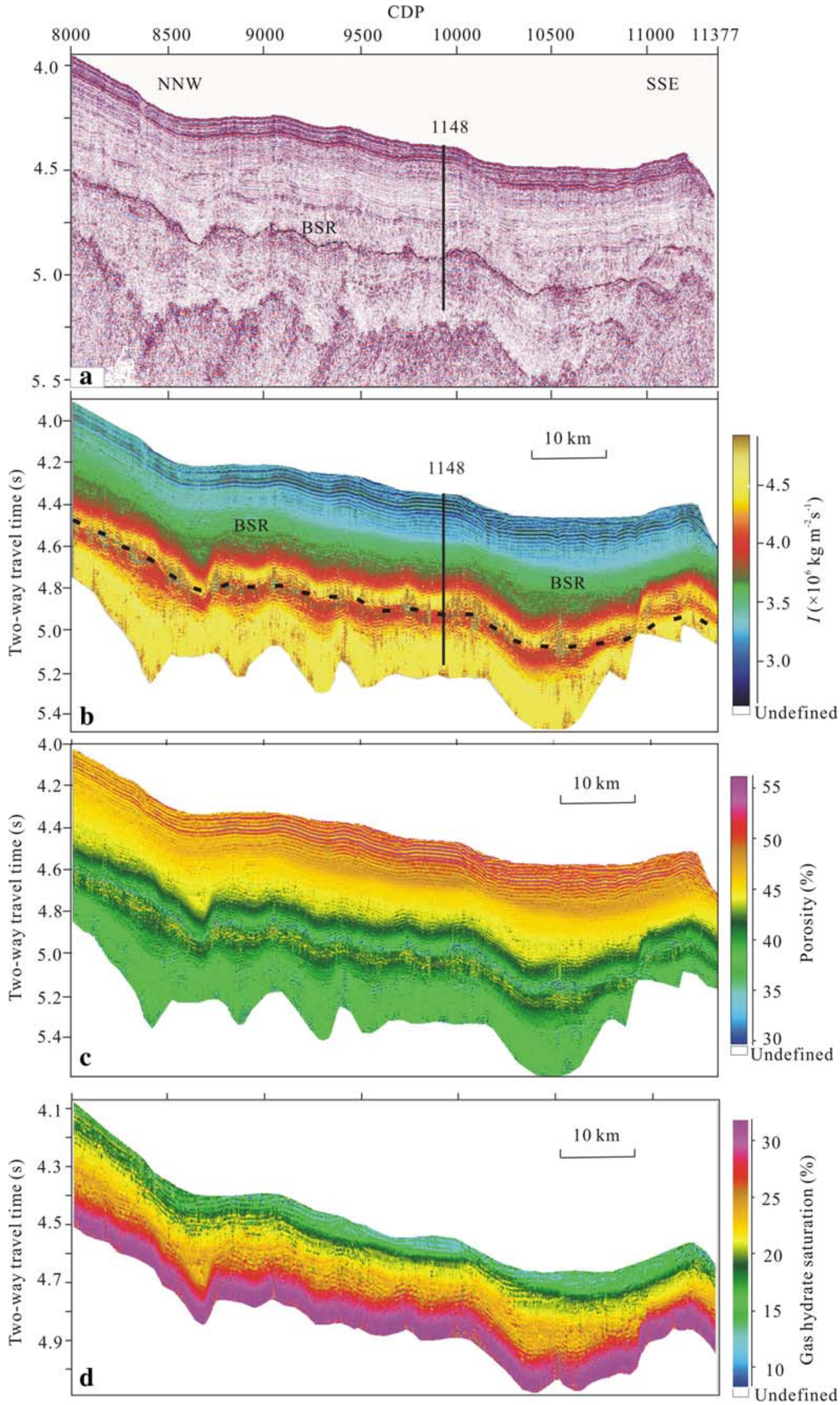
CDP
8000
8500
9000
9500
10000
10500
11000
11377
NNW
SSE
1148
BSR
a
b
c
d
10 km
Two-way travel time (s)
I (×10^6 kg m^-2 s^-1)
Undefined
Porosity (%)
Gas hydrate saturation (%)

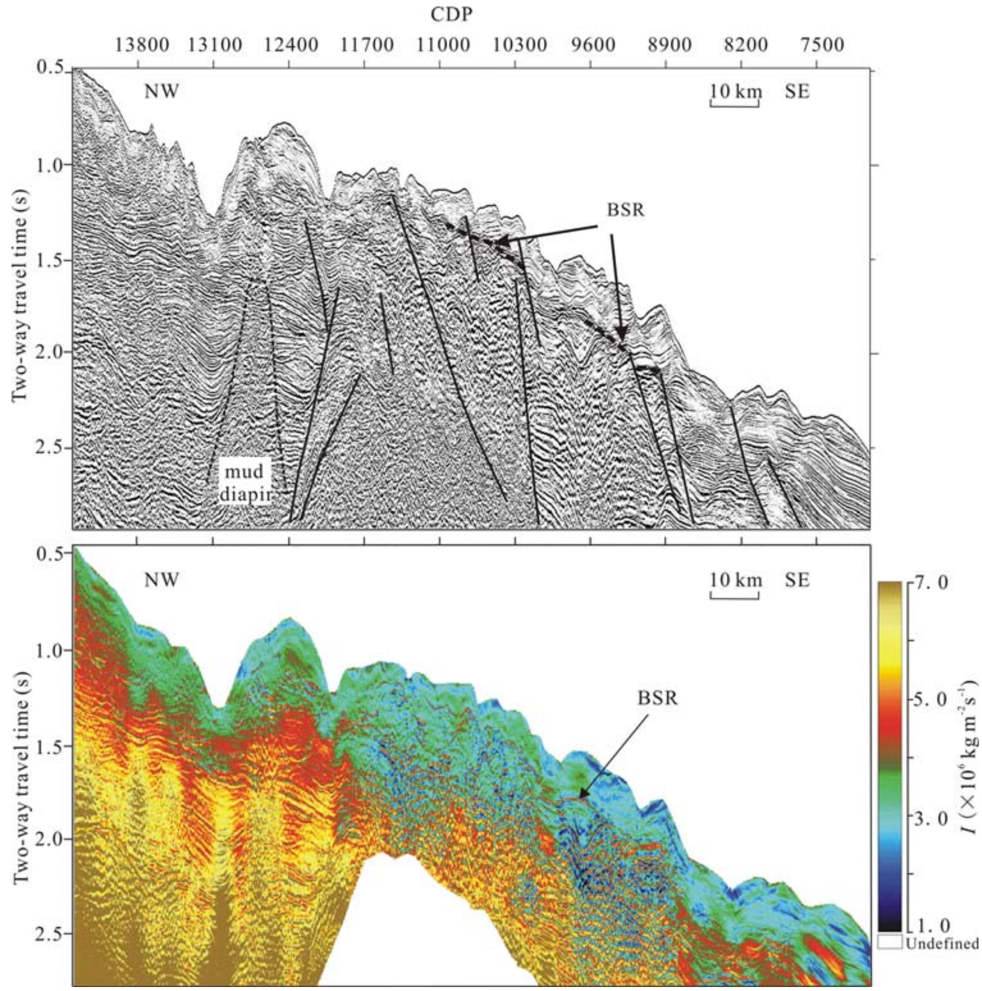

Fig. 4 (**a**) Part of seismic profile 0102 across the northern slope of the South China Sea. Note the complex mud diapir structure, active faults and BSR interpreted on this profile; (**b**) the acoustic impedance distribution obtained by CSSI. See Fig. 1 for profile location

known procedures (Ecker et al. 1998; Carcione and Tinivella 2000). A BSR is formed by the impedance contrast between the gas hydrate-bearing layer and the underlying free gas-bearing sediments. Lu and McMechan (2004) demonstrated that gas hydrate and free gas concentrations can be estimated from the acoustic impedance using the procedure of constrained sparse spike inversion (CSSI), which is based on seismic data and low-frequency impedance information obtained from well data. Although strictly speaking this technique does not depend on well data, the precision of the results does depend somewhat on the number of wells used. The inversion of seismic data to obtain acoustic impedance for the northern South China Sea was performed with the CSSI package of Jason Geosystems. Since seismic data are band-limited, the CSSI acoustic impedance data have abundant low-frequency information, which can be obtained from the low-frequency trends in the impedance logs of wells. These trends can be interpolated and extrapolated to the entire study area by following control horizons.

CSSI determines the acoustic impedance within prescribed constraints by minimizing the objective function

$$F_{\text{obj}} = \sum (r_i)^p + \lambda^q \sum (d_i - s_i)^q \quad (5)$$

at time i, where r_i is the reflection coefficient, d_i the recorded seismic trace, s_i the synthetic trace, p and q empirically determined exponents, and λ the data mismatch weighting factor. The match between output impedance and seismic data is determined by λ. If λ is lower than the ''true'' value, then the match between the synthetic trace and the recorded seismic data worsens and the output impedance is very approximate. As λ approaches its ''true'' value, the match improves and the output impedance provides a better description of the physical properties of the sediment. The value of λ is optimized for signal-to-noise, correlation misfit, seismic misfit and reflectivity misfit.

For the inversion of seismic line 0101, we used $\lambda = 20$, $p = 1$ and $q = 2$. Wave velocity, porosity, resistivity, density and impedance information were obtained from drilling results at ODP Site 1148 (Shipboard Party 2000). In the CSSI, both the low-frequency and high-frequency information are obtained from well downhole geophysical logging data. The input includes the time-migrated seismic data, the seismic wavelet, the interpolated control horizons and the interpolated low-frequency impedance trend. The acoustic impedance is then derived using CSSI (Fig. 3b). Below the gas hydrate zone, the acoustic impedance of the sediment is higher than that of gas-bearing sediments, suggesting that free gas is scarce in this zone (Figs. 3b and 5e).

Estimation of the degree of gas hydrate saturation

The formation of gas hydrates changes the physical properties of the sediment. The most readily observable change is an increase in seismic velocity, which is proportional to gas hydrate concentration (Pearson et al. 1983). Ecker et al. (2000), for example, used spatial variations in seismic velocity to estimate the spatial variations in gas hydrate concentration. Another change is an increase in acoustic impedance, which has been used in rock type classification and as an indirect hydrocarbon indicator (Latimer et al. 2000).

Gas hydrate-bearing sediments are characterized by high resistivity and velocity anomalies. If we assume that the resistivity anomalies are caused by the presence of gas hydrate in the sediments and that the pore space is filled with water and gas hydrate, then the gas hydrate saturation S_h is given by Archie's equation (1942):

$$S_h = 1 - S_w = 1 - \left(\frac{R_0}{R_t}\right)^{\frac{1}{n}} \quad (6)$$

where S_w is water saturation, R_0 is the resistivity of the water-saturated sediment, R_t the measured formation resistivity and n an empirical constant. For gas hydrate-bearing sediments, n = 1.9386 (Pearson et al. 1983). We assume that the background resistivity R_0 is constant along the entire seismic line and that for ODP Site 1148, R_0 is derived by a linear least-squares regression with depth (dashed line in Fig. 5a):

$$R_0 = 0.9716 + (3.801 \times 10^{-4})z \quad (7)$$

where z is the depth below seafloor in meters. The gas hydrate concentration above the BSR can now be obtained from Eqs. 6 and 7 (Fig. 5b).

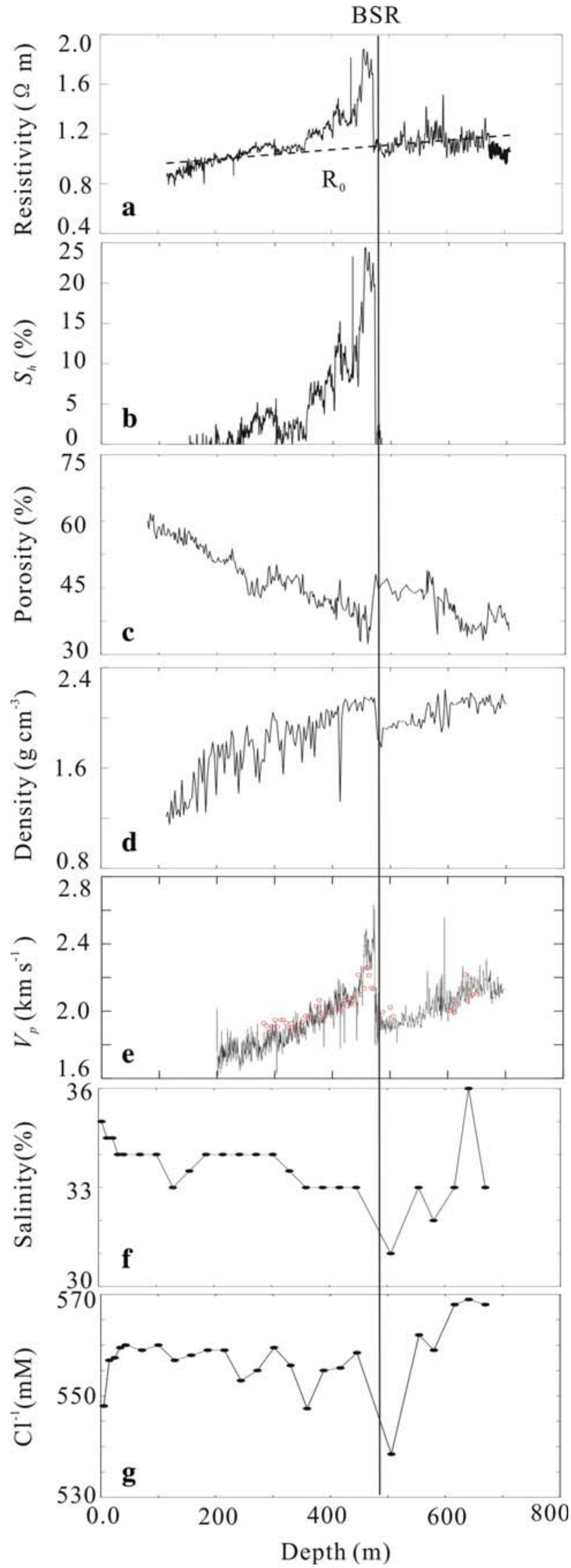

Fig. 5 Well logs from ODP Site 1148. The dashed line in the resistivity log refers to the water-saturated formation resistivity (R_0). Red circle refers to water-saturated P-velocity. The vertical solid line denotes the location of the BSR. Depth (d) is in metres below the seafloor

The relationship between gas hydrate saturation S_h, water-filled porosity ϕ and resistivity of the water-saturated formation (R_0) and of the pore water (R_w) is given by (Lu and McMechan 2002):

$$S_h = 1 - \left(\frac{R_0\phi^m}{aR_w}\right)^{\frac{1}{n}} \tag{8}$$

where R_0, R_w, and the constants m, a and n are determined empirically for a particular environment. In Eq. 8, the only unknown is ϕ. Thus, if the relationship between acoustic impedance (I) and water-filled porosity (ϕ) is known, the gas hydrate saturation can be estimated using Eq. 8.

Assuming that compaction of the sediment without gas hydrate and free gas is uniform, the relationship between acoustic impedance and water-saturated porosity will be a smooth curve along which ϕ decreases and I increases with increasing depth. The presence of gas hydrates in the sediment causes a decrease in ϕ and an increase in I. In contrast, the presence of free gas results in a decrease in both ϕ and I. In a gas hydrate-bearing zone, deviations from the water-saturated ϕ *vs.* I curve line is a measure of gas hydrate saturation, which also corresponds to the deviation of resistivity from the resistivity of water R_0 (Fig. 5a).

To obtain the relationship between water-filled porosity and acoustic impedance for the northern South China Sea, logging data from ODP Site 1148 were used. The gas hydrate-bearing zone was located by anomalies in resistivity, acoustic impedance, chloride concentration and compressional velocity. The ϕ *vs.* I curve was then derived using a polynomial least-squares fit of the logging data (Fig. 6):

$$\phi = -2.717I^3 + 33.205I^2 - 142.278I + 253.443 \tag{9}$$

where ϕ is neutron porosity in%, and I is acoustic impedance in 10^6 kg m^{-2} s^{-1}.

The porosity values were derived from the acoustic impedance data using Eq. 9 (Fig. 3c), and the gas hydrate saturation section was estimated using Eqs. 8 and 9 (Fig. 3d) with $m = 2.56$, $a = 1.05$ and $n = 1.936$ (Pearson et al. 1983). Not surprisingly, gas hydrate saturation obtained by inversion of the seismic data agrees very well with that derived from the resistivity log at ODP Site 1148.

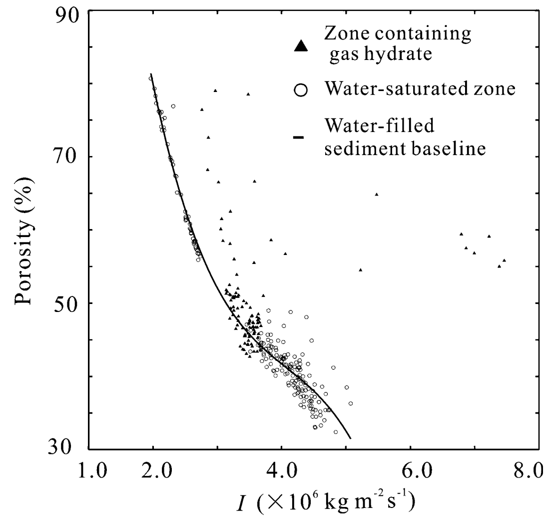

Fig. 6 Cross plot of porosity vs. acoustic impedance for ODP Site 1148

Discussion

Depth of BSR

BSRs were observed beneath the southeastern slope of the Dongsha Islands in the South China Sea at ODP Site 1146 (Zhu et al. 2003). Chloride concentrations (Cl^{-1}) in interstitial waters at ODP Site 1148 are relatively constant between 39 and 458 mcd, and only decrease slightly toward the base of the interval (Fig. 5g). Below 458 mcd, Cl^{-1} decreases to 548 mM similar to surface and then increases to a maximum of 577 mM near the base of the hole. Cl^{-1} is higher than observed at ODP Site 1146. The interstitial water salinity is similar. Below 458 mcd, salinity changes greatly (Fig. 5f). Sulfate (SO_4^{-2}) concentrations decrease, while SO_4^{-2} increases slowly between 120 and 518 mcd. Sulphate values never reach zero, indicating that methanogenesis is not an important process in the sediments. High methane values at the base of the drilled section are related to thermogenic production of hydrocarbons (Wang et al. 2000). The BSR at ODP Site 1148 is difficult to correlate with the well log data. The base of the hydrate stability zone calculated by heat flow and thermal conductivity is 305 mcd. There are small changes in resistivity, porosity, P-velocity and density at this depth, though the carbonate content is high.

In contrast, Song et al. (2001) suggested that the BSR at ODP Site 1148 is located at about 475 m depth. Resistivity, bulk density, velocity comes to a maximum, while Cl^{-1} and porosity decrease a minimum (Fig. 5), which may indicate presence of gas hydrates. However, colour spectral reflectance (CSR) measurements from split-core surfaces increase (L*) and decrease (a*/b*). The concentration of carbonate reaches 76%, so that a sharp increase in P-velocity, the bulk density and low porosity may be explained by the increased carbonate content in this interval (50–75 wt%). In this case lithology rather than gas hydrates would be responsible for prominent double reflectors in the seismic reflection profile line 0101 at 4.9 s (Wang et al. 2000). The mineral constituents and their contents of ODP Site 1148 were studied by Jiang (2006) from 50 to 700 mcd. The sediment solid phases include quartz, clay, carbonate and feldspar. The elastic constants of the solid phase are calculated from those of the individual mineral constituents using Hill's (1952) average formula. We calculated compressional wave velocity by an effective medium model for the elastic moduli offered by Dvorkin et al. (1999). The input parameters include the porosity, mineral constituents and their relative proportions, together with the physical properties of individual mineral constituent. The P-velocity of water-saturated sediment can be obtained if we assume that the sediment is full of water (Fig 5e). Though the P-velocity from ODP Site 1148 reaches 2.13 km/s at 470 mcd due to the high carbonate content, the P-velocity is still higher by about 0.28 km/s than the water-saturated P-velocity. The polarity is opposite to that of the seafloor and is caused not only by a change in the carbonate content but also by the presence of gas hydrate.

Tectonic constraints for BSR occurrence

BSRs are widespread in the Xisha Trough, southwest of the Dongsha Islands and in the vicinity of the Taixinan Basin of the northern South China Sea at water depths between 600 and 3000 m (Fig. 1). The amplitudes in the Taixinan Basin are low in comparison with typical BSRs (Liu et al. 2006), and their occurrence is controlled by seafloor morphology, local structure and the presence of active fluid transport.

Between the Shenhu uplift and the Zhu II depression (Fig. 1) is a wide fault zone with a steep bottom gradient. The Paleogene sequences in the depression are the main targets for hydrocarbon exploration because they are rich in methane. Some of the Upper Cretaceous-Paleogene faults were still active in the Neogene and Quaternary (Lüdmann and Wong 1999). They provide good passageways for the migration of gas-bearing fluids and thus promote favourable conditions for the formation of gas hydrates. At the same time, the subaqueous fan facies close to the main fault zone are coarse, making them good hydrocarbon reservoir rocks. Thus, large volumes of gas-bearing fluids could migrate upwards along this fault zone and become trapped in the coarse-grained rocks. Gas hydrates would then form where the gas hydrate stability zone is reached (Wang et al. 2003).

The sedimentary environment is another important factor governing BSR occurrence. The distinct BSRs about 200–450 ms beneath the uneven seafloor on seismic line 0102 are associated with large submarine landslides and slumps at water depths of 1200–1660 m on the northeastern Dongsha Rise (Fig. 4a). Occasional blanking zones are also visible.

Cause for low-amplitude BSRs: lower gas hydrate concentrations *vs.* scarcity of free gas beneath the gas hydrate stability zone

Whether free gas is present in the sediment underlying the gas hydrate stability zone has been hotly debated (Dillon and Paull 1983; Hyndman and Spence 1992; Singh et al. 1993). Low- as well as high-amplitude BSRs have been observed in the northern South China Sea, for example on seismic lines 0101 and 0102 respectively. On line 0101, free gas is absent beneath the gas hydrate zone (see Figs. 3 and 5, and Sect. 3.2), and the BSR is indistinct. On seismic line 0102, the structures are complex and the strata below the BSR is discontinuity (Fig. 4a). The BSR is much more easily recognizable from acoustic impedance. The acoustic impedance is high above the BSR, while acoustic impedance is low below (Fig. 4b), which indicates that free gas is probably present. This observation also suggests that BSRs are enhanced by the presence of free gas below the gas hydrate stability zone because of the increased acoustic impedance contrast.

Many methods are available to evaluate the degree of gas hydrate saturation in sediments. Kaster et al. (1995) used well logging velocity and Vertical Seismic Profiling of velocity sections to estimate gas hydrate concentrations on the Cascadia margin of western Canada. Their values from ODP Site 899 vary from 11 to 20%. For ODP Sites 994, 995 and 997 on the Blake Ridge, the same method yielded gas hydrate concentrations of 3.9, 5.7, and 5.8% respectively (Paull et al. 1996). The corresponding values at ODP Sites 994 and 997 that were determined using oxygen isotopic fractionation and $\delta^{18}O$ anomalies of the interstitial waters are 6 and 12% respectively (Matsumoto et al. 2000). Ecker et al. (2000) used spatial variations in seismic velocity to estimate the spatial variations in gas hydrate concentration. Estimates of gas hydrate saturation on the Blake Ridge and offshore southern California range from 50% of the pore space using the time average equation (Wood et al. 1994; Yuan et al. 1996) to 10–15% using the weighted equation (Lee et al. 1996). Our estimates of the degree of gas hydrate saturation in the northern South China Sea based on the equation of Archie (1942) are 3–25% in the pore space. These values are comparable to those from other oceanic areas and are also consistent with the high acoustic velocities that exist in the northern South China Sea. The high acoustic velocities may be caused by high carbonate content. We suggest therefore that low concentrations of gas hydrates is not the main reason for the low amplitudes of the BSRs on the seismic profiles 0101, but rather the scarcity of free gas below the gas hydrate stability zone and variation in the sediment mineralogy.

The cause of this gas scarcity is still a matter of speculation. Methane carbon isotope ratios indicate that most of the methane at ODP Site 1148 is biogenically derived (Zhu et al. 2003). Kvenvolden (1993) proposed the in situ biogenic methane production and supply model, according to which disseminated methane hydrate formation can take place anywhere within the stability field. Continuous sediment loading and compaction induces fluid advection, and sedimentation supplies organic carbon continuously resulting in in situ methane production. Although gas hydrate can be generated in the entire gas hydrate stability zone according to the model of Kvenvolden (1993), the maximum pore volume occupancy by methane hydrate without vertical methane-rich fluid migration from greater depths is probably less than 5–10% (Rempel and Buffet 1997). To account for our maximum gas hydrate concentration of about 20%, we invoke the role played by extensional fracturing, which might have provided passage-ways for methane gas migration. Syn-sedimentary faulting was very important during Cretaceous-Paleogene rifting, and some of these faults were still active during the Miocene-Quaternary, although their Miocene offsets are more difficult to accurately quantify (Fig. 3a). Studies elsewhere have shown that active faulting strongly influences the migration of gas and the accumulation of both gas hydrate and free gas (McDonnel et al. 2000; Paull et al. 1996; Paull and Dillon 2001). An additional cause for gas scarcity is the low total organic carbon (TOC) content in the sediments below the BSR. For example, at ODP Site 1148 TOC only reaches 0.2–0.5 wt%, with a maximum of about 1 wt% (Leventhal 2004). This low TOC results in low methane productivity. The scarcity of free gas below the gas hydrate stability zone and upward gas migration along the (active or inactive) extensional fractures to the gas hydrate stability zone to form gas hydrates left little free gas below the gas hydrate stability zone, so that the BSR amplitudes are low.

Accuracy and limitations of the method

Our estimates of the degree of gas hydrate saturation in the northern South China Sea are based on a combination of Archie's equation and an indirect empirical estimation of porosity from acoustic impedance. The values of R_w and R_0 in Eq. 8 were determined for the South China Sea, but n, m and a were assumed to be the same as those for the Blake Ridge (Pearson et al. 1983). This is the most important source of error. With these five parameters known, gas hydrate saturation is reduced to a function of porosity. The estimation of gas hydrate concentrations from seismic lines using the procedures above is therefore at best approximate, even though the values can be 'calibrated' using appropriate well logging data. Thus, the values presented in this paper should be treated with caution.

Conclusions

Structural elements (such as faults and fractures) and seafloor morphology are important factors controlling the distribution of BSRs in the northern South China Sea. Local active faults, mud diapirs and coarse sedimentary facies provide favourable conditions for the formation of gas hydrates and with it the occurrence of BSRs.

Gas hydrate-bearing sediments have high acoustic impedance and these impedance anomalies are controlled primarily by the degree of gas hydrate saturation, which can be determined using Archie's equation. The gas hydrate concentrations at ODP Site 1148 are estimated to be 3–25% of the pore space. These estimates are less than those derived from seismic data, which lie within the range of 10–30%. Our results suggest that in the northern South China Sea, gas hydrate saturation is high in the gas hydrate stability zone, but free gas is scarce beneath this zone. It is the scarcity of free gas that has led to the low amplitudes of the BSRs.

Acknowledgements We would like to thank the Guangzhou Marine Geological Survey for their permission to release the data used in this paper. We would like to thank the help of Peter Clift, Paula Sonneveld and all the reviewers. I also thank Junhua Guo for help in drafting the figures. The research work reported here was supported by the 863 program (2006AA09A209-6), the Innovation Project of CNPC (W060123) and the Knowledge Innovation Project of CAS (KZCX3-SW-219).

References

Anderson RN, Langseth MG, Hayes DE, et al (1978) Heat flow, thermal conductivity. A Geophysical Atlas of east and southeast Asian Seas, Char Ser. MC-25. Hayes ed. Geol. Soc. of Am. Boulder, Colo., USA, pp. 1–125

Andreassen K (1995) Seismic studies of a bottom simulating reflection related to gas hydrate beneath the continental margin of the Beaufort Sea. J Geophys Res 100(B7):12659–12673

Archie GE (1942) The electrical resistivity log as an aid in determining some reservoir characteristics. J Petr Tech 5:1–8

Briais A, Patriat P, Tapponnier P (1993) Updated interpretation of magnetic anomalies and seafloor spreading stages in the South China Sea: implications for the tertiary tectonics of Southeast Asia. J Geophys Res 98:6299–6328

Carcione JM, Tinivella U (2000) Bottom-simulating reflectors: seismic velocities and AVO effects. Geophysics 65:54–67

Chi WC, Reed DL, Liu CS, Lundberg N (1988) Distribution of the bottom simulating reflector in the offshore Taiwan collision area. Terrestrial Atmospheric Ocean Sciences 9:779–794

Clift PD, Lin J (2001) Preferential mantle lithospheric extension under the South China margin. Mar Petrol Geol 18:929–945

Clift PD, Lin J, Barckhausen U (2002) Evidence of low flexural rigidity and low viscosity lower continental crust in the South China Sea. Mar Petrol Geol 19(8):951–970

Clift PD (2006) Controls on the erosion of Cenozoic Asia and the flux of clastic sediment to the Ocean. Earth Planet Sci Lett 241:571–580

Dai JC, Xu HB, Snyder F, Dutta N (2004) Detection and estimation of gas hydrates using rock physics and seismic inversion: Examples from the northern deepwater Gulf of Mexico. TLE 23(1):60–66

Dickens GR, Quinby-hunt MS (1994) Methane hydrate stability in seawater. Geophys Res Lett 21:2115–2118

Dillon WP, Paull C (1983) Marine gas hydrates, II—Geophysical evidence. In: Cox JL (ed) Natural Gas Hydrates: Properties, Occurrences and Recovery: Butterworths, pp. 73–90

Dvorkin J, Parasad M, Sakai A, Lavoie D (1999) Elasticity of marine sediments: Rock physics modeling. Geophys Res Lett 26(12):1781–1784

Ecker C, Dvorkin J, Nur A (1998) Sediments with gas hydrates: Internal structure from seismic AVO. Geophysics 63:1659–1669

Ecker C, Dvorkin J, Nur A (2000) Estimating the amount of gas hydrate and free gas from marine seismic data. Geophysics 65:565–573

Egeberg PK (2000) Hydrate associated with fluid flow above salt diapir (site 996). In: Paull CK, Matsumoto R, Wallace PJ, Dillon WP (eds) Proceedings of the ODP, Scientific Results, 164:219–228

Hill R (1952) The elastic behaviour of crystalline aggregate. Proc Physical Soc London A65:349–354

Huang CY, Wu WY, Chang CP, et al. (1997) Tectonic evolution of accretionary prism in the arc-continent collision terrane of Taiwan. Tectonophysics 281:31–51

Hyndman RD, Spence GD (1992) A seismic study of methane hydrate marine bottom simulating reflectors. J Geophys Res 97(B5): 6683–6698

Hyndman RD, Davis E (1992) A mechanism for the formation of methane hydrate and seafloor bottom simulating reflectors by vertical fluid expulsion. J Geophys Res 97(B5):7025–7041

Jiang HY (2006) The composition and fluxes of sedimentary minerals at ODP Site 1148 and their response to tectonic movements. Dissertation, Institute of Oceanology, Chinese Academy of Sciences

Jin C, Wang J (2002) A preliminary study of the gas hydrate stability zone in the South China Sea. Acta Geoloica Sinica 76(4):423–428

Kastner M, Sample JC, Whiticar MJ, Hovland M, Cragg BA, Parkes JR (1995) Geochemical evidence for fluid flow and diagenesis at the Cascadia convergent margin. In: Carson B, Westbrook GK, Musgrave RJ, Suess E (eds) Proc. ODP, Sci. Results, 146 (Pt 1): College Station, TX (Ocean Drilling Program), pp. 375–384

Kvenvolden K (1993) Gas hydrates –geological perspective and global change. Reviews of Geophysics 31:173–187

Latimer RB, Davison R, Riel PV (2000) An interpreter's guide to understanding and working with seismic-derived acoustic impedance data. The Leading Edge 19:242–256

Lee MW, Hutchinson DR, Collet TS, Dillon WP (1996) Seismic velocities for hydrate-bearing sediments using weighted equation. J Geophys Res 101:20347–20358

Lee MW, Hutchinson DR, Agena WF, Dillon WP, et al. (1994) Seismic character of gas hydrates on the southeastern U.S. continental margin. Marine Geophysical Researches 16:163–184

Lee TY, Lawver LA (1995) Cenozoic plate reconstruction of Southeast Asia. Tectonophysics, 251:85–138

Leventhal JS (2004) Isotopic chemistry of organic carbon in sediment from Leg 184. In: Prell WL, Wang P, Blum P, Rea DK, Clemens SC (eds) Proc. ODP, Sci. Results, pp.184:1–13

Liu CS, Schnürle P, Wang Y, et al. (2006) Distribution and characters of gas hydrate offshore of southwestern Taiwan. Terr Atmos Ocean Sci 17(4):615–644

Lu S, McMechan GA (2002) Estimation of gas hydrate and free gas saturation, concentration, and distribution from seismic data. Geophysics 67:582–593

Lu S, McMechan GA (2004) Elastic impedance inversion of multichannel seismic data from unconsolidated sediments containing gas hydrate and free gas. Geophysics 69:164–179

Lüdmann T, Wong HK (1999) Neotectonic regime on the passive continental margin of the northern South China Sea. Tectonophysics 311:113–138

Lüdmann T, Wong HK, Wang PX (2001) Plio-Quaternary sedimentation processes and neotectonics of the northern continental margin of the South China Sea. Marine Geology 172:331–358

Matsumoto R, Borowski WS (2000) Gas hydrate estimates from newly determined oxygen isotopic fractionation (''GH-IW'') and $\delta^{18}O$ anomalies of the interstitial waters: Leg 164, Blake Ridge. In: Paull CK, Matsumoto R, Wallace PJ, Dillon WP (eds) Proc. ODP, Sci. Results, 164:59–66

McConnell DR, Kendall BA (2003) Images of the base of gas hydrate stability in the deepwater Gulf of Mexico: Examples of gas hydrate traps in northwest Walker Ridge and implications for successful well planning. TLE 22(4):361–367

McDonnel SL, Max MD, Cherkis NZ, Czarneeki MF (2000) Tectono-sedimentary controls on the likelihood of gas hydrate occurrence near Taiwan. Marine and Petroleum Geology 17:929–936

Milkov AV (2000) Worldwide distribution of submarine mud volcano and associated gas hydrates. Geophys J Int 167:29–42

Milkov AV, Claypool GE, Lee YJ, et al. (2003) In situ methane concentrations at Hydrate Ridge, offshore Oregon: New constraints on the global gas hydrate inventory from an active margin. Geology 31(10):833–836

Minshull TA, Singh SC, Westbrook GK (1994) Seismic velocity structure at a gas hydrate reflector, offshore western Columbia, from full waveform inversion. J Geophys Res 99:4715–4734

Paull CK, and Dillon WP (eds.) (2001) Natural Gas Hydrate: Occurrence, Distribution and Detection. Am. Geophys. Union Monogr. Ser., No. 124, 53–66

Paull CK, Matsumoto R, Wallace PJ, and the Leg 164 Scientific Party (1996) Proceedings of the Ocean Drilling Program, Initial Report, 164, p. 318

Pearson CF, Halleck PM, McGuire PL, et al. (1983) Natural gas hydrate: A review of in situ properties. J Phys Chem 87:4180–4185

Rempel A, Buffet B (1997) Formation and accumulation of gas hydrate in porous media. J Geophys Res 102:10151–10164

Ru K, Pigott JD (1986) Episodic rifting and subsidence in the South China Sea. AAPG Bull 70:1136–1155

Shi XB, Qiu XL, Xia KY, Zhou D (2003) Characteristics of surface heat flow in the South China Sea. Journal of Asian Earth Sciences 22:265–277

Shipley TH, Houston MH, Buffler RT, et al. (1979) Seismic evidence for widespread possible gas hydrate horizon on continental slopes and rises. AAPG Bull 63:2204–2213

Singh SC, Minshull TA, Spence GD (1993) Velocity structure of a gas hydrate reflector. Science 260:204–207

Sloan ED (1998) Clathrate hydrates of natural gases. second edition. Marcel Dekker Inc., New York, p. 628

Song H, Matsubayashi O, Kuramoto S (2001) Processing of seismic data of western nanhai trough and its characteristic bottom simulating reflector. Chinese J Geophys, 44(6):799–804

Song H (2003) Geophysical researches on gas hydrates. Ocean Press, Beijing, p. 174

Taylor B, Hayes DE (1983) Origin and history of the South China Sea. In: Hayes DE (ed) The Tectonic and Geologic Evolution of Southeast Asian Seas and Islands, Part 2, AGU Geophysical Monograph 27:23–56

Wang H, Zhang G, Yang M, Liang JQ, et al. (2003) Tectonic environment of gas hydrates on the northern slope of the South China Sea. Mar Geol Quaternary Geol 23(1):81–86 (in Chinese)

Wang PX, Prell WL, Blum P, Arnold EM, Bühring C, Chen MP, Clemens S, Clift P, Colin C, Farrell J, Higginson M, Leventhal J, Li A, Su X, Shyu JP, McIntyre K (2000) Exploring the Asian monsoon through drilling in the South China Sea. Proc Ocean Drill Prog: Initial Rep 184:1–77

Wood WT, Stoffa PL, Shipley TH (1994) Quantitative detection of methane hydrate through high-resolution seismic velocity analysis. J Geophys Res 99:9681–9695

Wu S, Zhang G, Huang Y, Liang J, Wong HK (2005) Gas hydrate occurrence on the northern slope of the South China Sea. Mar Petrol Geol 22(1):403–412

Yao B (1998) Preliminary survey of gas hydrates in northern South China Sea. Mar Geol Quaternary Geol 18(4):11–18 (in Chinese)

Yao B (2001) Gas hydrates in the South China Sea. Trop Oceanol 20(2):20–28 (in Chinese)

Yuan T, Hyndman RD, Spence GD, Desmons B (1996) Seismic velocity increase and deep-sea hydrate concentration above a bottom-simulating reflector on the northern Cascadian slope. J Geophys Res 101:13655–13671

Zhang GX, Huang YY, Zhu YH, Wu BH (2002) Prospect of gas hydrate resources in the South China Sea. Mar Geol Quaternary Geol 22(1):75–81 (in Chinese)

Zhu Y, Huang Y, Matsumoto R, and Wu B (2003) Geochemical and stable isotopic compositions of pore fluids and authigenic siderite concretions from Site 1146, ODP Leg 184: implications for gas hydrate. In: Prell WL, Wang P, Blum P, Rea DK, Clemens SC (eds) Proc. ODP, Sci. Results, 184:1–15